SAXS Studies on Structural Changes in a Poly(vinyl alcohol) Film during Uniaxial Stretching in Water

Tsukasa Miyazaki,*,† Akie Hoshiko,† Midori Akasaka,† Takuji Shintani,† and Shinichi Sakurai‡

Core Technology Center, Nitto Denko Corporation, 1−1−2, Shimohozumi, Ibaraki, Osaka 567-8680, Japan, and Department of Polymer Science & Engineering, Kyoto Institute of Technology, Matsugasaki, Sakyo-ku, Kyoto 606-8585, Japan

Received December 4, 2005; Revised Manuscript Received March 2, 2006

ABSTRACT: We have investigated structural changes in a poly(vinyl alcohol) (PVA) film during uniaxial stretching in water by conducting simultaneously the tensile stress−strain measurement with small-angle X-ray scattering (SAXS) using our newly developed drawing apparatus for the in situ SAXS measurements. Below the strain of 70%, the crystalline lamellae orient to the direction perpendicular to the stretching direction and the intervening amorphous regions are elastically expanded with the film drawing in proportion to the macroscopic deformation. Beyond the strain of 70%, the molecular chains in the intermediate amorphous region are relaxed with the lamellar breakup. Above 180% strain, the structural transition of the lamellar structure to the microfibrillar one takes place, as suggested by appearance of the transversal streak with an intensity maximum on each streak and the mechanical transition. Moreover, interfibrillar interaction of the adjacent microfibrils decreases with the film stretching by the pulling-out of the tie chains, which are interpenetrating to the adjacent microfibrils, leading to the macroscopic plastic deformation of the PVA film and stress relaxation of most of the microfibrils, which is shown by the continuous longitudinal long period decrease. In the final stage of deformation, the networking with a long-range connectivity composed of the microfibrils and the interfibrillar extended amorphous chains proceeds associated with the sliding between the adjacent microfibrils with successive drawing. However, the network of the interfibrillar extended amorphous region is considered to be an origin of the strain-induced hardening, which occurs above 180% strain up to a break, because most of the microfibrils are relaxed with strain.

1. Introduction

Recently, liquid crystalline displays (LCD) have been widely used in various industrial applications such as televisions, monitors of cellular phones, and so on. Poly (vinyl alcohol) (PVA) has been promising as a substrate of polarizers used in LCD. PVA films are very suitable to the application to polarizers because they possess a high ability of PVA−iodine complex formation in the film microstructure.[1] When PVA films are soaked in a KI/I_2 aqueous solution, adsorbed iodines are one-dimensionally (1-D) aligned along with the orientation of PVA chains by the film drawing, followed by the formation of PVA−iodine complexes, which show an extremely high ability of dichromatic performance.

About 10 years ago, Miyasaka et al. systematically investigated the microstructure of PVA−iodine complexes in the films.[2] They also proposed a structural model of a PVA−iodine complex, on the basis of their experimental result that PVA−iodine complexes are preferentially formed in the amorphous region rather than the PVA crystalline phase, upon soaking PVA films in KI/I_2 aqueous solution at relatively low iodine concentrations usually used in the preparation of polarizers.[2,3] In their model, the one-dimensional arrays of polyiodines are surrounded to some extent with extended PVA amorphous chains. Extension of PVA films remarkably enhances the PVA−iodine complex formation, implying that the model of the PVA−iodine complex proposed by Miyasaka et al. seems to be reasonable compared to other models previously proposed, such as the helix model.[4,5] A similar model was proposed by Takamiya et al., who suggested that polyiodines are surrounded with the aggregates of extended syndiotactic sequences in the PVA chains.[6]

PVA films are extremely swollen with water, allowing the film to be drawn up to a high draw ratio as high as 7−8 times depending on the molecular weight of films. The molecular chains highly orient to the stretching direction, with the film stretching in a highly drawing regime. Polyiodine complexes absorbed in the amorphous regions are considered to be highly oriented to the polymer chain direction associated with the film stretching. The higher dichromatic performance is attained when the draw ratio is higher. Therefore, the formation of polyiodine complexes should be closely related to the microstructure of PVA films in the course of drawing in water, especially to that in the amorphous region, leading to the detailed investigation of the microstructural changes in PVA films associated with the film stretching in water.

For a structure model of PVA films in water, Miyasaka et al. also proposed the "*Double network model*" as schematically shown in Figure 1.[2,7]

They supposed that the PVA film consists of microfibrils, in which the crystalline lamellar and the amorphous region alternatingly stack, with the amorphous region between microfibrils (not shown in Figure 1). Moreover, they assumed that the amorphous layer in the lamellar structure contains tie chains that interconnect crystallites. As there are two networks in their model, a polymer chain network and a fibrillar network, it is referred to as a double-network model. Prior to their studies, the similar model was proposed by Apostolov and Fakirov for other polymer systems.[8] We previously reported the micro-

* To whom correspondence should be addressed. E-mail: tsukasa_miyazaki@gg.nitto.co.jp. Telephone: +81-72-621-0265. Fax: +81-72-621-0316.

† Core Technology Center, Nitto Denko Corporation.

‡ Department of Polymer Science & Engineering, Kyoto Institute of Technology.

10.1021/ma052595u CCC: $33.50
Published on Web 03/24/2006

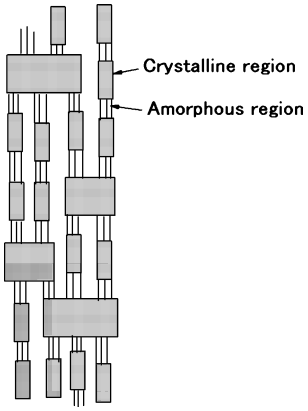

Figure 1. Schematic diagram of a structural model for the PVA film stretched in water. The amorphous region between the microfibrils is not shown in the figure.

structure of PVA films dried in an air oven after stretching in water.[9] The network model similar to the one proposed by Miyasaka et al. could explain our obtained results well.

In this article, we present the preliminary results on the structural changes in PVA films during uniaxial stretching in water for elucidating the structural model in the stretched PVA films in further detail by using simultaneous measurements of small-angle X-ray scattering (SAXS) and the tensile stress−strain relationship. It is expected that this study leads to the development of a polarizer with high dichromatic performance.

2. Experimental Section

2.1. PVA Films. The PVA films made by Kuraray Co. (Vinylon) with the degree of polymerization of 2400 were used in this study. The triad tacticity ($mm = 0.21$, $mr = 0.50$, $rr = 0.29$) was determined in solution state by ^{1}H NMR spectroscopy. The films also had a high degree of saponification, which is larger than 99 mol %. The thickness of the PVA films was 0.075 mm.

2.2. Tensile Testing. The stress−strain curves for the films in water were obtained by a tensile testing apparatus (AUTO GRAPH AG-100E, Shimadzu Corp.) with a specially designed homemade water bath for the investigation of the films in water. Rectangular-shaped specimens of gauge dimensions 10×15 mm^2 in the dried state were examined.

2.3. SAXS Measurements. SAXS experiments were performed with the SAXS apparatus at BL40B2 and BL45XU beamlines of SPring-8 (Japan Synchrotron Radiation Research Institute, Hyogo, Japan). The wavelength of X-rays was turned at 0.1 and 0.09 nm for the SAXS experiments at BL40B2 and BL45XU, respectively. The camera length of the SAXS apparatus was about 1500 mm and 2000 mm, respectively. On both experiments, the CCD detector system bearing an image intensifier was used to allow a rapid scan of two-dimensional (2-D) SAXS patterns from the samples during uniaxial stretching in water. The calibration of the scattering angle was carried out by using diffraction from a regular structure in collagen obtained from chicken tendon.

2.4. Newly Developed Stretch Machine for SAXS Measurements. Simultaneous SAXS and stress−strain experiments were performed at the BL40B2 beamline with our newly developed stretch machine. A schematic drawing of the stretch machine is shown in Figure 2a. This stretch machine allows a film sample to be stretched symmetrically in the lateral direction, which assured that the X-ray beam always illuminated the same position of the sample during stretching. A load cell is mounted on one side of the shaft. The load cell and an encoder linked to a motor allowed us to measure a stress−strain curve during uniaxial stretching of the film. The film width used in this experiment was 20 mm. The initial length of the film of 30 mm can be extended up to 270 mm, indicating that the film can be stretched up to 800% strain. Moreover, this instrument is equipped a water bath that can be jacked up and down so as to enclose and disclose the film specimen, respectively, as shown in Figure 2a. The water bath has holes for the beam path, which are covered with two polyimide windows with a thickness of 25 μm. The gap between the two polyimide windows is 1 mm, in which water and the film is placed, as schematically shown in Figure 2b for the top view of the water bath.

The gap of 1 mm was determined by taking account of two factors: the absorption of X-rays by water is increased for a larger gap, while the smooth stretching of the film in the gap is limited for a shorter gap. The temperature of water can be controlled in a range from room temperature to 373 K by using a temperature controller with an accuracy of $\pm$ 1 K. The selected stretching speed was 5 mm/min (17% strain/min). Two-dimensional SAXS patterns were accumulated every acquisition period of 15 s by using the CCD detector along with a drawing. Therefore, a 2-D SAXS pattern is attributed to an averaged structure during deformation in 15 s. The 2-D SAXS pattern measured for water was subtracted as a background noise without transmittance correction because the transmittance of the samples in water is identical to that of water background. To analyze structures parallel and perpendicular to the stretching direction, the 2-D SAXS pattern was sector-averaged respectively along the longitudinal and transversal directions within a sector angle allowance $\pm$ 5 deg. This obtained 1-D profile (scattering intensity $I(q)$ as a function of the magnitude of the scattering vector q defined by $q = (4\pi/\lambda) \sin \theta/2$ with λ and θ being the wavelength of X-rays and the scattering angle, respectively) was further subjected to the so-called Lorentz correction, i.e., $q^2I(q)$ is plotted as a function of q. It is well-known that the above Lorentz correction is only applicable to isotropic systems. However, this correction can be conventionally applied to partially oriented systems, as suggested by Ruland.[10] In fact, this correction was adopted in many cases of uniaxial systems.[11−13] As mentioned below, in our case, we must continuously investigate the structural parameters of the film at low strains including the isotropic one and at relatively large strains during uniaxial deformation. In particular, the main features of the structural changes of the film

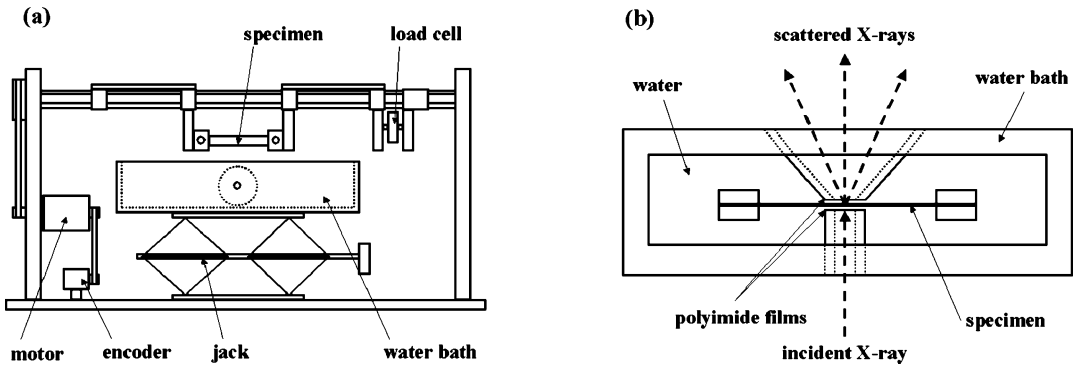

Figure 2. (a) Schematic drawing of the newly developed stretch machine for in situ SAXS measurements during uniaxial deformation of PVA films in water. (b) The top view of the water bath.

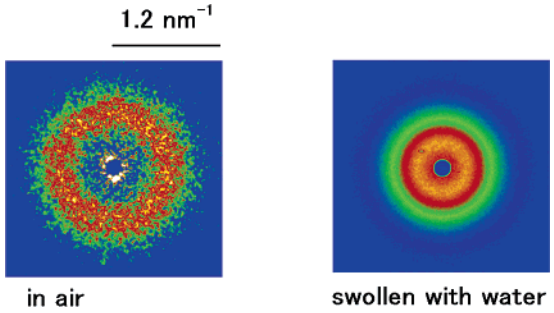

Figure 3. Two-dimensional small-angle X-ray scattering pattern for the same film in air and in water. The patterns obtained in air and in water were corrected for the air scattering and the water scattering background, respectively.

during uniaxial stretching are shown in low strain regions. Therefore, the same correction should be used for all data, including that obtained in the isotropic state and in strained ones for excluding systematic errors.

For the preliminary and convenient examination of the samples swollen with water before drawing or at relatively low strains, a different stretching apparatus was used at BL45XU. Continuous stretching is not available with this apparatus. Instead, several fixed positions are provided for the sake of sample cramps, which enables 2-D SAXS measurements at selected strains by manually drawing the sample in water.

3. Results

3.1. Swelling Behavior of PVA Films with Water. First, we performed the preliminary study on the swelling behavior of the PVA films with water at the BL45XU beamline. The typical examples of the 2-D SAXS patterns of the same film without film stretching in air and in pure water are shown in Figure 3. For the undeformed samples, a circular scattering pattern with a homogeneous intensity distribution along the circle is observed in air and in water, as expected from the randomly oriented stacks of the crystalline lamellar embedded in an amorphous matrix. However, the long period derived from the scattering pattern substantially increases in water compared with that in air, indicating that the film sample is swollen with water.

We examined azumuthally integrated 1-D scattering profiles as a function of the swelling time. Data acquisition time was 1.5 s. The correlation function analysis[14] is adopted to quantitatively analyze the lamellar structure in the swollen film. The correlation function $\gamma(r)$ is calculated from the scattering intensity as

$$\gamma(r) = \frac{\int_0^\infty I_{cor}(q) \cos(q \cdot r)\, dq}{Q} \quad (1)$$

where $I_{cor}(q)$ is the Lorentz-corrected intensity, which is given by multiplying the observed intensity by q^2, and Q is the invariant defined as

$$Q = \int_0^\infty I_{cor}(q)\, dq \quad (2)$$

The typical example of the correlation function is shown in Figure 4 for the film in water at the swelling time of 150 s.

The position of the first maximum (d_{max}) in the 1-D correlation function corresponds to the long period (lamellar periodicity), while the position of the first minimum (d_{min}) very closely corresponds to the lamellar crystalline thickness or the intermediate amorphous region thickness.[15,16] Figure 5 shows

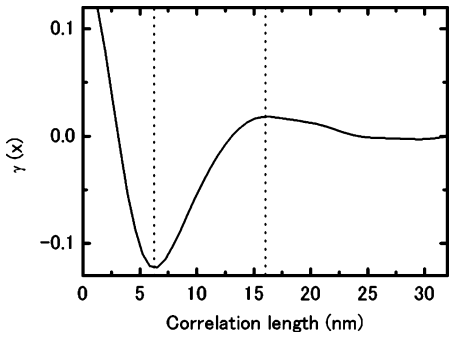

Figure 4. Typical example of the 1-D correlation function for the film swollen in water at the swelling time of 150 s.

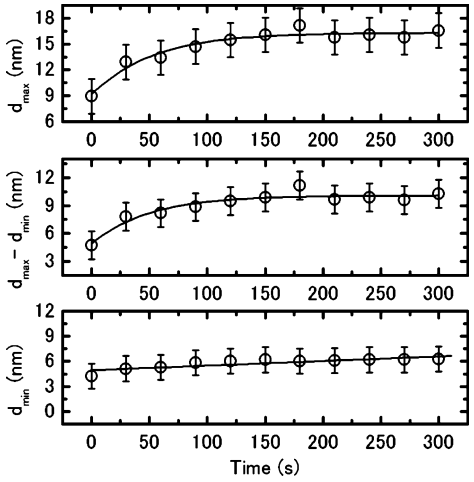

Figure 5. One-dimensional correlation function results for the film swollen in water as a function of the swelling time. d_{max} and d_{min} indicate the positions of the first maximum and the first minimum in the 1-D correlation function, respectively. $d_{max} - d_{min}$ is the difference between both positions.

d_{max}, d_{min}, and their difference ($d_{max} - d_{min}$), with the swelling time for the film swollen with pure water.

d_{max} increases immediately on the immersion of the film in water, while d_{min} remains constant, implying that the increase in the long period is attributed to the extension of $d_{max} - d_{min}$. It is naturally inferred that d_{min} and $d_{max} - d_{min}$ should be assigned to the crystalline and the amorphous layer thickness, respectively, and that only the amorphous regions are swollen with water on the basis of the same increasing trend of d_{max} and $d_{max} - d_{min}$. There are two reasons why the above assignments are reliable.

First, we examined the wide-angle X-ray scattering profile of the PVA film in water. It was concluded that the scattering profile from the crystalline region is not affected with water when the scattering profile of water is merely subtracted from the whole scattering profiles. These indicate that the crystalline region must not be swollen with water and not be dissolved in water. Other authors were led to the same conclusion.[17,18] This indicates that d_{min} should be assigned to be the crystalline thickness.

Second, for PVA films in water, if only the amorphous region is swollen with water while the crystalline layer does not absorb water, the electron density deference between the two phases increases, and consequently, the scattering invariant also increases. The scattering invariant increases in the same trend as d_{max} and $d_{max} - d_{min}$, as shown in Figure 6, indicating that the electron density difference between the lamellar crystalline and the amorphous region increases in water. We attempt to estimate the increase in the scattering invariant on the assump-

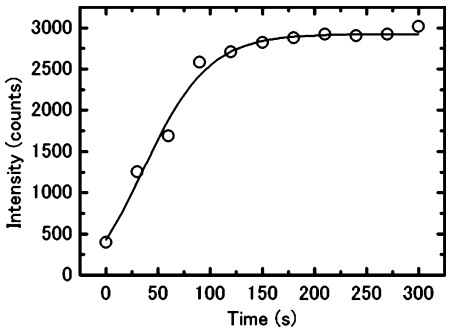

Figure 6. Invariant of the scattering intensity from the film swollen in water as a function of the swelling time.

tion that only the amorphous region is swollen with water, while the crystalline region does not absorb water. The scattering invariant can be described as follows,[19]

$$Q \propto \phi_c(1-\phi_c)(\rho_c-\rho_a)^2 \tag{3}$$

Here, ϕ_c, ρ_c, and ρ_a are the crystallinity of the polymer, the electron density of the crystalline, and the amorphous layer, respectively. By using eq 3, the ratio of Q for the fully swollen state of the film to Q_0 for the dried state can be described as follows,

$$\frac{Q}{Q_0} = \frac{\lambda}{(\rho_c-\rho_a)^2\{\phi_c+\lambda(1-\phi_c)\}^2}\cdot\left\{\rho_c-\frac{\rho_a+\lambda-1}{\lambda}\right\}^2 \tag{4}$$

Here, λ is the swelling ratio. ρ_c and ρ_a are normalized with the electron density of water. The swelling ratio is defined by the ratio of the amorphous region thickness swollen with water to the dried one. The electron density of the swollen amorphous region is assumed to be the averaged value with that of water according to the swelling ratio. For the amorphous layer thickness in the fully swollen state, λ is about 2.5, as shown in $d_{max} - d_{min}$ in Figure 5. In a previous paper, we estimated the crystallinity of the film to be 0.34.[9] As shown in Figure 6, Q/Q_0 is about 7, consistent with the value of 6.2, calculated using eq 4 with $\lambda = 2.5$ and $\phi_c = 0.34$. These indicate that our conclusion that only the amorphous region is swollen with water, while the crystalline region does not absorb water, can explain well the increase in the scattering invariant in the swollen state of the film compared to the one in the dried state.

The scattering invariant of the fully swollen film with water was examined for 30 min in water, and it was found that the scattering invariant remains constant, indicating that the crystalline regions are not swollen with water in the experimental time scale at least. The swelling with water is saturated in 2 or 3 min on the immersion of the film in water, as shown in Figures 5 and 6. In the following sections, the tensile stretching of the film will be performed after 3 min on the immersion of the film in water for the examination of the films in the equilibrated state.

3.2. Tensile Testing of PVA Films. A typical stress−strain curve and the derivative of it are shown in Figure 7a and b, respectively, similar to the stress−strain curve of the cross-linked rubber with an ability of strain-induced crystallization. The nominal stress was calculated from the load at each strain and the cross section of an initial film without swelling with water. The initial elastic region is very narrow and the defined yield point has not appeared. The strain-induced hardening occurs prior to the break of the film. Figure 7b indicates that the strain-induced hardening occurs at the strain of about 200%.

The same tensile testing device was also used to investigate the elastic-recovery properties of the stretched samples at different stages of the deformation process. The film sample is stretched step-by-step with a constant speed of 10 mm/min. After each step, the stretching speed is inverted and used to contract the sample until a stress of zero is achieved. The remaining strain at this point represents the plastic part, ϵ_p, of the total strain, ϵ_t, and the difference between the total and the plastic strains give the elastic part, ϵ_e.[20,21] The test sample is extended again by using the same strain speed up to the initial strain value before contracting, whereupon another step is performed again under the constant strain speed. This allows the same test sample to be used for more than one cycle.

Figure 8a presents the result of a step-cycle test for the PVA film in water. For comparison, the result of the continuous stretching run indicated with a dashed line is also included. It is found to agree with the series of steps, indicating that the interruption by the cycles does not affect the stretching properties. Strobl et al. suggested that various mechanical transition points are deduced from the composition of ϵ_p and ϵ_e carried out at various ϵ_t's described as the true strain (Hencky strain).[20,21] The results of this composition are shown in Figure 8b. At a relatively low strain, ϵ_e is substantially larger than ϵ_p. However, ϵ_e becomes constant above ϵ_t of about 1 (corresponds to the nominal strain of about 180%) while the increase in ϵ_p is facilitated. It was suggested that the onset of the constant elastic part corresponds to the onset of fibrillation processes in many semicrystalline polymers.[20−24] As shown in Figure 7b, the strain-induced hardening occurs near by this nominal strain of 180%, also indicating that the structural changes such as the structural transition of the lamellar structure to the microfibrillar one must occur at the critical strain of 180% as an origin of the strain-induced hardening.

3.3. In Situ SAXS Measurements during Uniaxial Deformation. A stress−strain curve and typical 2-D scattering patterns obtained simultaneously during uniaxial deformation in water at 298 K are shown in Figure 9. Each arrow drawn from the 2-D patterns to the stress−strain curve in the figure indicates the strain at which the 2-D pattern was obtained. The stress−strain relationship completely follows the stress−strain behavior obtained with the tensile testing device shown in Figure 7a and b. The selected longitudinal and transversal slices derived from the 2-D SAXS patterns are shown in Figure 10a and b with various strains, respectively. The arrows in these figures indicate the sequential traces of the peak position with strain for clarification, which describe the changes of the long period and the scattering intensity. Moreover, the long periods evaluated from each slice by using the Bragg's law, $2\pi/q$, are shown in Figure 11a and b. Interesting 2-D SAXS patterns and the consequent longitudinal and transversal long periods could be obtained at each strain region.

In the elastic region below the strain of about 70%, the scattering intensity is enhanced in the direction parallel to the stretching direction, indicating that the lamellar crystallites orient perpendicular to the stretching direction. The orientation direction of the lamellar is consistent with that of the films stretched in water and followed by air-drying.[9] The detailed mechanism of the lamellar orientation in this region will be elucidated in the near future when our planned wide-angle X-ray scattering study will be performed by using the same experimental setup.

In this region, the longitudinal long period substantially increases with strain, as shown in the shift of the maximum position in the longitudinal 1-D scattering profiles to a lower q

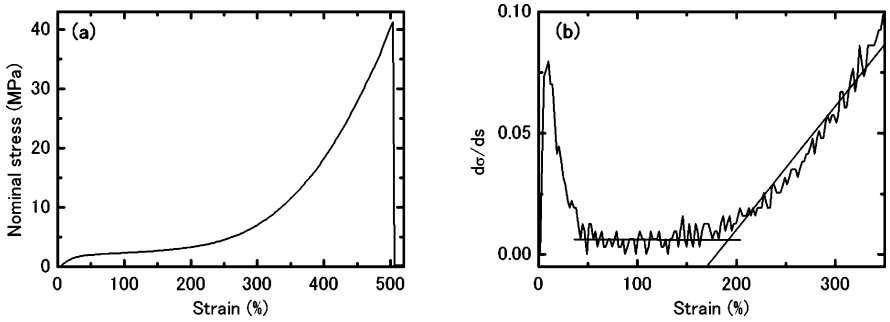

Figure 7. Stress−strain relationship of the PVA film (a) and the derivative (b) at 298 K, using a tensile testing device (AUTO GRAPF) with a homemade water bath.

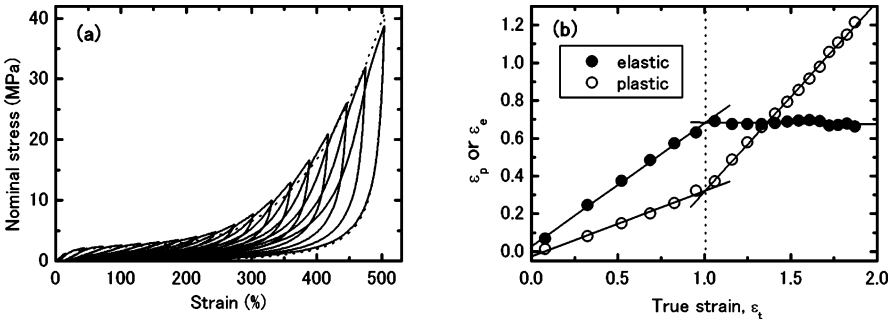

Figure 8. (a) Step-cycle test carried out for the PVA film in water. (b) Evolution of the step-cycle test on the sample: the elastic (ϵ_e) (closed circles) and the plastic (ϵ_p) (open circles) for the true total strain (ϵ_t).

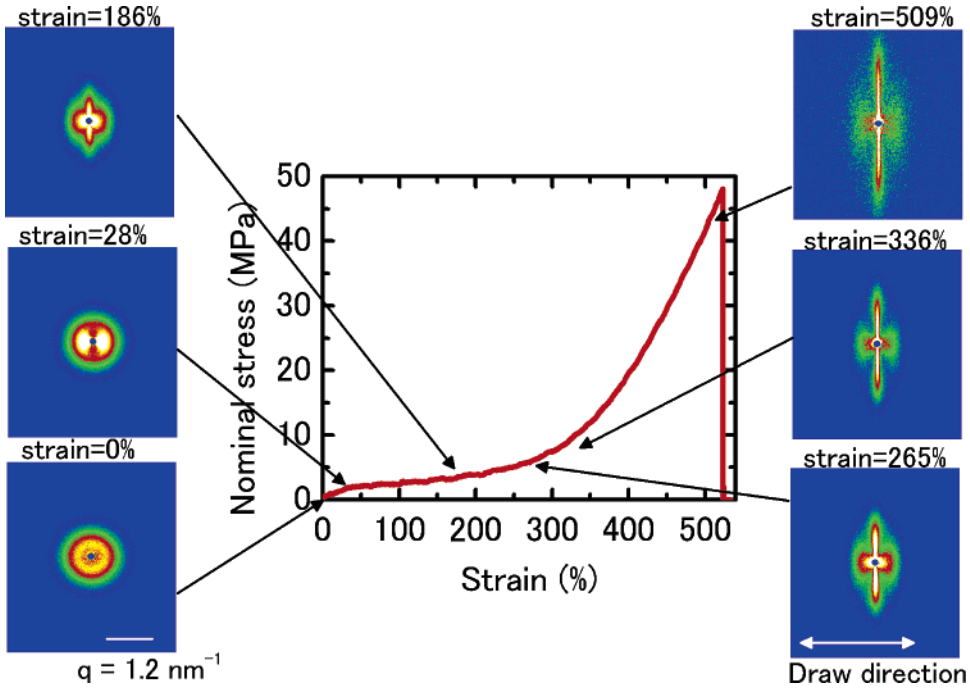

Figure 9. Stress−strain curve and typical 2-D SAXS patterns collected during uniaxial deformation in water at 298 K. Each pattern was obtained in 15 s from the point indicated by each arrow.

value, which is indicated in Figure 10a by the arrow, and this is indicated directly in Figure 11a. In addition, the increase in the scattering intensity should be associated with the lamellar orientation, as mentioned above, and/or may be attributed to dilution of the intermediate amorphous phase with strain, which leads to an increase in the density difference between the crystalline and the amorphous region. The inset of Figure 11a shows an expanded view of the early portion of the longitudinal long periods up to 70% strain for the detailed investigation of the substantial increase in the longitudinal long period. Because the straight line in the inset of Figure 11a is drawn on the assumption that the long period is proportional to the macroscopic strain of the film, the lamellar structure in the PVA film in water is concluded to be deformed up to 70% strain in proportion to the macroscopic strain in the stretching direction. In this region, the longitudinal long periods can reversibly decrease, going through nearly the same path indicated in the inset of Figure 11a, when the film is contracted. Therefore, it is considered that the increase in the long period with strain should be attributed to the elastic expansion of the amorphous layers, which leads to the macroscopic elastic behavior of the film at a relatively low strain (Figure 8b). When the deformation

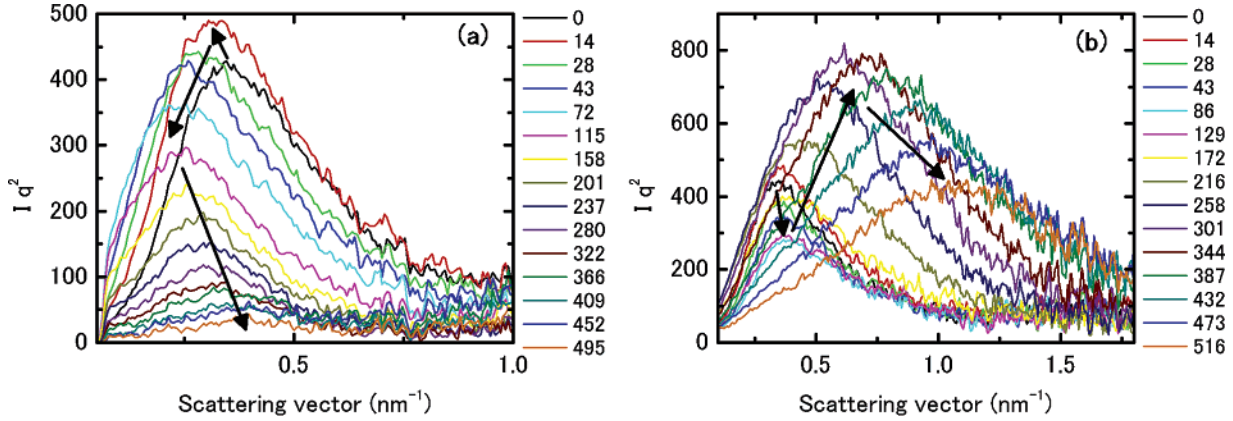

Figure 10. Selected longitudinal 1-D slices (a) and the transversal slices (b) of the 2-D SAXS patterns during uniaxial deformation in water at 298 K with the strain indicated in the figure. All data is not included for clarity. The arrows indicate the trend of the peak positions in each strain region.

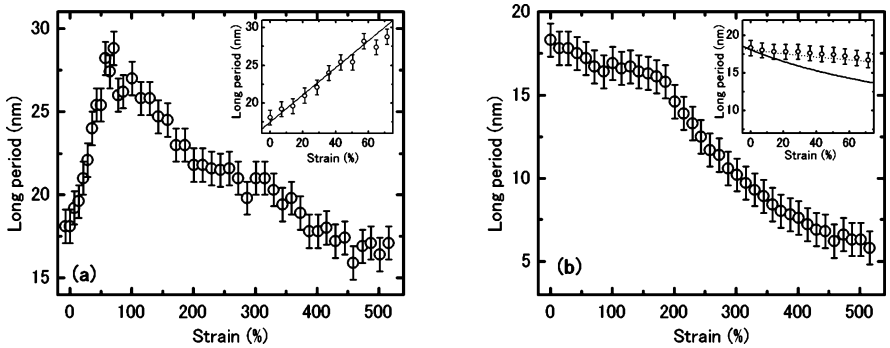

Figure 11. Long periods derived from the position of the maximum in the scattering profiles in the longitudinal (a) and the transversal (b) direction to the stretch direction in water at 298 K, using the Bragg's law, $2\pi/q_{max}$. The insets in each figure are expanded views of the early portion of the long period up to 70% strain. The solid lines in the insets are drawn on the basis of the affine deformation mechanism of the sample. The dotted line in the inset of Figure 11b indicates the deformation with the Poisson ratio of 1/6.

proceeds with the volume constant of the film, it can be generally expected that the longitudinal and the transversal long periods obey the affine deformation mechanism. In Figure 11b, the transversal long period gradually decreases with strain, as expected from the deformation of the sample with the longitudinal uniaxial stretching. However, the decrease in the lateral long period is much lower than the one expected by the affine deformation mechanism, which is shown in the inset of Figure 11b with the solid line.

Above 70% strain, the longitudinal long period increase is followed by the decrease with strain, as shown in Figure 11a, indicating that the amorphous region can be no more extended with strain. This decrease in the longitudinal long periods should be attributed to relaxation of the amorphous region due to the lamellar breakup prior to the microfibrillation, as shown in our previous result on the large reduction in the transversal crystallite size between the draw ratios of 1 (the strain of 0%) and 2 (the strain of 100%) for the dried film after stretching in water.[9] In Figure 11b, the transversal long period gradually decreases with strain up to 180% strain. Through this region, substantial reductions of the longitudinal and the transversal scattering intensity were observed with strain, which is mainly due to the decrease in the scattering volume associated with the sample stretching and/or may be due to the destruction of some lamellar crystals, as shown in Figure 10a and b.

Above 180% strain, an intense streak scattering appears in the transversal direction in the 2-D SAXS patterns of Figure 9 and in these transversal slices in Figure 10b. This streak scattering moves to a higher q value with strain, as indicated with an upward arrow in Figure 10b, implying that the correlation length in the transversal direction decreases with increasing the strain. In Figure 11b, rapid reductions of the transversal long period were observed above the strain of 180%, associated with the appearance of this intense streak scattering in the transversal direction. The origin of this streak scattering should be the interparticle distance between the microfibrils in the drawn films rather than microvoids or cracks,[12,25] as shown in our previous paper for the dried films after the stretching in water,[9] because there is a peak in the streak scattering, as shown in Figure 10b (the 1-D slices in this figure are Lorentz-corrected intensity profiles, but a peak can be detected in the uncorrected ones).

Of course, the peak in the streak scattering may possibly correspond to an approximate intervoid distance associated with the longitudinal void growth with strain. However, the origin of the streak scattering must be the same as the one observed in our previous paper for the dried films after stretching in water. If the streak scattering from the stretched film in water is attributed to the intervoid distance, the intensity of the streak scattering must be relatively smaller than that in a dried state because of the smaller electron density difference between the swollen polymer matrix and water compared with the one between the dried polymer matrix and air. Nevertheless, the intensity of the transversal streak scattering is relatively larger than that in a dried state, as shown in Figure 9 in this study and Figure 2 in our previous paper. Therefore, we concluded that the transversal streak scattering should be attributed to the interparticle distances between the microfibrils.

The transition of the lamellar structure to the microfibrillar one takes place at the strain 180%, as shown in the appearance of transversal streak scattering. This strain of 180% is consistent with the one at which the fibrillation and the strain-induced

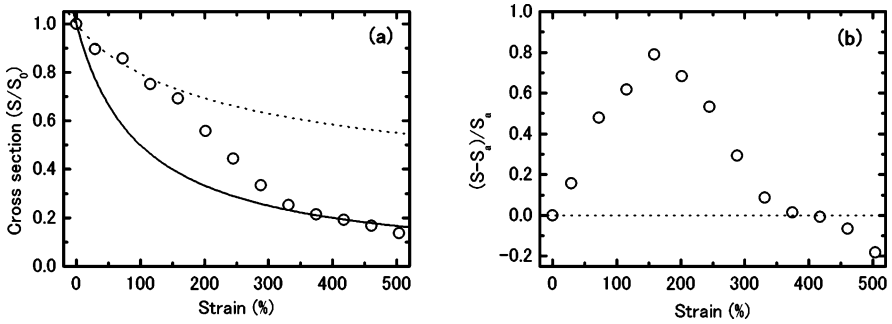

Figure 12. (a) Cross section of the film normalized with the one at the strain of 0%. The solid line and the dotted line are the cross section calculated on the assumption of the deformation with the Poisson ratio of 0.5 and 1/6, respectively. (b) Ratio of the difference between the measured cross section of the film and the one calculated on the assumption of the deformation with the Poisson ratio of 0.5 to the calculated one.

hardening begin to occur, as suggested with the step-cycle test and the stress−strain relationship, respectively (Figure 8a, b). Whereupon, each microfibril becomes to be packed tightly beyond the strain of 180%, which is indicated by the decrease in the interparticle distance between the microfibrils in Figure 11b, while the longitudinal long period continuously decreases. This tightly packing of the microfibrils must be induced with the onset of the networking including the microfibrils with a long range connectivity associated with the sliding between the adjacent microfibrils. The enhancement of the macroscopic plastic flow indicated in Figure 8b is thought to originate from this sliding between the adjacent microfibrils in this region. That is to say, the network that bears the stress with the film stretching through a long range connectivity begins to be developed successively with fibrillation above the strain of about 180%. Moreover, with the development of the network, the strain-induced hardening occurs, as shown in Figure 7b.

4. Discussion

4.1. Transversal Long Period Decrease at the Low Strain Region. As mentioned above, when the deformation proceeds with the volume constant of the film, it can be generally expected that the longitudinal and the transversal long periods obey the affine deformation mechanism. However, at the low strain, the transversal long period decrease with strain is much lower than the one expected by the affine deformation mechanism, which is shown by the solid line in the inset of Figure 11b. For the further detailed investigation related to the macroscopic lateral dimension of the film, we measured the cross section of the film with strain, as shown in Figure 12a. The cross section of the film at each strain is normalized with the one obtained at the strain of 0%. The solid line in this figure is drawn on the basis of the affine deformation mechanism, which is the deformation with the Poisson ration of 0.5. Actual decrease in the cross section of the film is much lower than the expected one, especially in the relatively low strain region up to the strain of 150−200%, indicating that the deformation does not proceed with the volume constant of the film. This lower volume decrease must be correlated to water flow to the inside of the film in the time scale of experiment. For the estimation of water volume in the film with strain, we plot the ratio of the difference between the measured cross section of the film and the one calculated on the assumption of the deformation with the Poisson ratio of 0.5 to the calculated one in Figure 12b. This figure shows that the strain-induced swelling of the film with water occurs up to the strain of 150−200%.

Takigawa et al. investigated the swelling behavior of gels with the uniaxial strain in good solvents.[26−28] They showed that the stress-induced swelling in the direction perpendicular and parallel to the stretching direction occurs in gels with uniaxial strain, implying that the deformation of gels may proceed with a lower Poisson ratio than 0.5. When a gel is stretched, the free energy of the gel system will change to attain a new equilibrium state under tension. The relaxation time for swelling is determined by the diffusion constant of the solvent and sample size of swelling gel systems. The swelling of the stretched gel also takes a long time until reaching the equilibrium size. They theoretically indicated that the deformation of gels proceeds with the Poisson ratio of 1/6 (osmotic Poisson ratio) if the experiment is performed in a long time beyond the relaxation time of the stress-induced swelling. The dotted line in Figure 12a shows the deformation of the film with the Poisson ratio of 1/6, indicating that the deformation at the relatively low strain can be represented by the deformation with the Poisson ratio of 1/6. Furthermore, the transversal long period decrease also follows the deformation with the Poisson ratio of 1/6, as shown by the dotted line in the inset of Figure 11b, implying that the lower decrease in the transversal long period with strain should be attributed to the stress-induced swelling of the film.

However, the same authors investigated the Poisson ratio of their PVA gels in solutions and showed that the PVA gels in good solvents have a Poisson ratio of about 0.5 within a wide experimental time scale, indicating that the relaxation times of the stress-induced swelling in the PVA gels are much longer than the experimental time scale usually used.[29] We believe that the difference in the relaxation time between our PVA film and their PVA gels used must be attributed to the initial structure of the films because the relaxation time is determined by the diffusion constant of water to the film,[26,27] which is predominated by the microstructure of PVA.

Interestingly, the stress-induced swelling of the film is substantially leveled off beyond the strain of 150−200%, as shown in Figure 12a and b. Consequently, the cross sections of the film above 300% strain fall on the solid line, calculated on the assumption of the deformation with the Poison ratio of 0.5, as shown in Figure 12a. The structural change from the lamellar structure to the microfibrillar one at about 180% strain mentioned above must be closely related to this drastic change of the swelling behavior of the film. Of course, further detailed investigations should be required for the stress-induced swelling behavior of the film used in related to the structural change with strain.

4.2. Reduction of the Longitudinal Long Period. Generally speaking, the transition of the lamellar structure to the microfibrillar one occurs during uniaxial deformation in a variety of semicrystalline polymers.[30−45] In many cases, including our case, the longitudinal long period decreases associated with the transition of the structure. For the explanation of this decrease

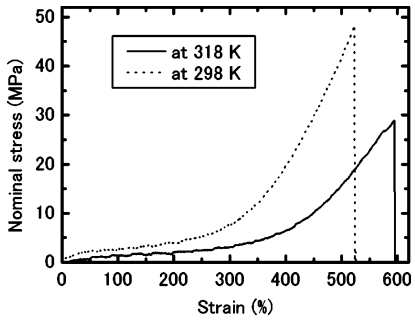

Figure 13. Stress−strain relationship of the PVA film obtained in water at 318 K. For comparison, the one obtained at 298 K is also included in this figure.

in the longitudinal long period, several models were proposed.[30−35] One of them is the melting and recrystallization model in the necking region.[32−34] Another model is the dislocation model.[35,36] As the other explanation of the reduction of the long period, relaxation of the original long period should be considered, as suggested by Fakirov et al. in the deformation behavior of drawn poly (ether ester) thermoplastic elastomers.[38−41] They suggested that the stretching of the sample leads to the elimination of the interfibrillar contacts because tie molecules that are interpenetrated to adjacent microfibrils are pulled out.

The structural transition associated with the large plastic flow by sliding between the adjacent microfibrils, such as our case, may be explained by the Fakirov's model. As indicated in our previous paper, the dried films after stretching in water show the continuous long period increase with the extension of the amorphous region only from the undrawn film to the highly drawn one, implying that the original structure remains essentially unchanged during deformation in water with the extension of the amorphous region, and no new structure with a different long period appears. Figure 13 shows the stress−strain relationship of the PVA film in water at 318 K obtained with our newly developed stretch machine. For comparison, the stress−strain curve obtained at 298 K is also included in this figure. The strain at the break increases compared with that of the film stretched in water at 298 K, whereas the stress at the break deceases. This should be attributed to relaxation of the polymer chains with higher mobility at a higher temperature. Parts a and b of Figure 14 indicate the simultaneous obtained structural parameters in the longitudinal and the transversal direction, respectively, in the same manner as Figure 11a and b. The transition to the microfibrillar structure suggested from the changes in the transversal long periods is delayed from 180% strain to about 300% strain, also attributed to relaxation of the polymer chains, as mentioned above. However, the initial and the final long periods in the longitudinal direction on stretching the film are nearly the same as the ones on stretching at 298 K, indicating that the decrease in the long period with the film stretching should not be attributed to a newly developed structure, such as that predicted by the melting and recrystallization model, because such a long period in a newly developed structure must be very sensitive to temperature during deformation.[33,34]

4.3. Strain-Induced Hardening with the Microfibrillar Networking. It is concluded that the fibrillation of the initial lamellar structure only occurs during uniaxial deformation according to the Fakirov's mechanism. Of course, the microstructure in the highly stretched film must be composed of the extended microfibrils and the interfibrillar extended amorphous chains for bearing the large stress applied to the film in the strain-induced hardening region. However, most of the microfibrils are relaxed with strain, as shown by the longitudinal long period decrease. The strain-induced hardening may occur with the network of the extended amorphous regions bearing the large stress in the film, as proposed by Prevorsek.[44,45] The network of these extended amorphous regions must play an important role in structuring of the PVA−iodine complexes, when the film is stretched in a KI/I_2 aqueous solution for the construction of a polarizer.

5. Conclusion

First, we studied the swelling behavior of the PVA film with water. For the PVA film in water, only the amorphous region is swollen with water, while the crystalline layer does not absorb water. Whereupon, we have investigated the structural changes of the PVA films during uniaxial deformation in water by the simultaneous measurements of stress−strain and SAXS by using our newly developed stretch machine, which allows a film sample to be stretched symmetrically in the lateral direction.

Below the strain of 70%, the crystalline lamellae orient to the direction perpendicular to the stretching direction and the intermediated amorphous regions are elastically expanded, with the film drawing in proportion to the macroscopic deformation, as expected from the swelling of the amorphous layers. Above the strain of 70%, the intermediated amorphous chains between the lamellae are relaxed with the lamellar breakup. Above the strain of 180%, the transition of the lamellar structure to the microfibrillar one takes place. Moreover, the sliding between the adjacent microfibrils and the consequent networking including the microfibrils, which is considered to be an origin of the macroscopic plastic flow of the film, occurs associated with the pulling out of the tie molecules interpenetrated to the adjacent microfibrils. Finally, the strain-induced hardening occurs with the development of the network of the extended amorphous regions bearing the large stress in the network because most of the microfibrils are relaxed with strain.

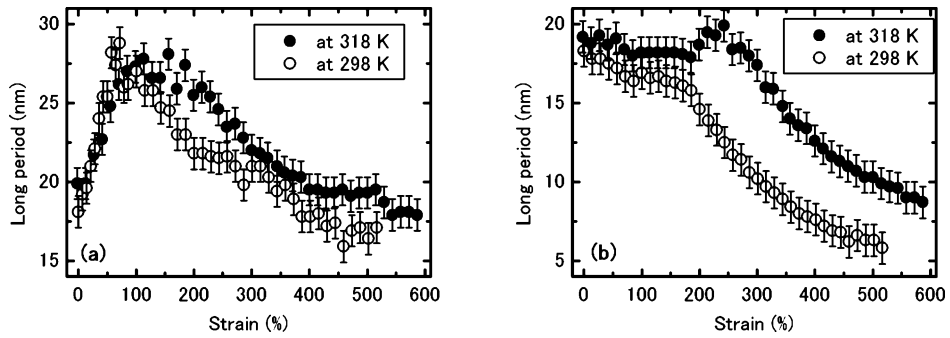

Figure 14. Long periods derived from the position of the maximum in the scattering profiles in the longitudinal (a) and the transversal (b) direction in water at 318 K. For comparison, the results obtained at 298 K are also included in this figure.

Acknowledgment. We wish to thank Dr. S. Sasaki and Dr. K. Inoue of the Japan Synchrotron Radiation Research Institute (JASRI), Y. Tsuji and Y. Yoshida of Kyoto Institute of Technology, Prof. K. Sakurai and Dr. I. Akiba of The University of Kitakyushu, and Dr. K. Yamamoto of Nagoya Institute of Technology for their support on our experiments at SPring-8. We also thank Prof. K. Tashiro of the Toyota Technological Institute for helpful discussions. The synchrotron radiation experiments were performed at the BL40B2 and the BL45XU in the SPring-8 with the approval of JASRI (proposal nos. 2004B0103-NL2b-np and 2005A0014-NL2b-np).

References and Notes

(1) Sakurada, I. *Polyvinyl Alcohol Fibers*; Marcel Dekker: New York, 1985.
(2) Miyasaka, K. *Adv. Polym. Sci*. **1993**, *108*, 91.
(3) Choi, Y. S.; Miyasaka, K. *J. Appl. Polym. Sci*. **1993**, *48*, 313.
(4) Zwick, M. M. *J. Appl. Polym. Sci.* **1965**, *9*, 2393.
(5) Inagaki, F.; Harada, I.; Shimanouchi, T.; Tasumi, M. *Bull. Chem. Soc. Jpn.* **1972**, *45*, 3384.
(6) Takamiya, H.; Tanahashi, Y.; Matsuyama, T.; Tanigami, T.; Yamaura, K.; Matsuzawa, S. *J. Appl. Polym. Sci.* **1993**, *50*, 1807.
(7) Kojima, Y.; Furuhata, K.; Miyasaka, K. *J. Appl. Polym. Sci.* **1985**, *30*, 1617.
(8) Apostolov, A. A.; Fakirov, S. *J. Macromol. Sci., Phys.* **1992**, *B31*, 329.
(9) Miyazaki, T.; Katayama, S.; Funai, E.; Tsuji, Y.; Sakurai, S. *Polymer* **2005**, *46*, 7436.
(10) Ruland, W. *Colloid Polym. Sci.* **1978**, *256*, 932.
(11) Hsiao, B. S.; Kennedy, A. D.; Leach, R. A.; Chu, B.; Harney, P. *J. Appl. Cryst.* **1997**, *30*, 1084.
(12) Samon, J. M.; Schultz, J. M.; Hsiao, B. S. *Polymer* **2000**, *41*, 2169.
(13) Ibanes, C.; David, L.; de Boissiel, M.; Seguela, R.; Epicier, T.; Robert, G. *J. Polym. Sci., Polym. Phys. Ed.* **2004**, *42*, 3876.
(14) Strobl, G. R.; Schneider, M. *J. Polym. Sci., Polym. Phys. Ed*. **1980**, *18*, 1343.
(15) Hsiao, B. S.; Sauer, B. B.; Verma, R. K.; Zachmann, H. G.; Seifert, S.; Chu, B.; Harney, P. *Macromolecules* **1995**, *28*, 6931.
(16) Samon, J. M.; Schulz, J. M.; Hsiao, B. S.; Seifert, S.; Stribeck, N.; Gurke, G.; Collins, G.; Saw, C. *Macromolecules* **1999**, *32*, 8121.
(17) Sakurada, I.; Nukushima, Y.; Mori, N. *Kobunshi Kagaku* **1955**, *12*, 302.
(18) Kanaya, T.; Ohkura, M.; Kaji, K.; Furusaka, M.; Misawa, M. *Macromolecules* **1994**, *27*, 5609.
(19) Vonk, C. G. In *Small-Angle X-ray Scattering*; Glatter, O., Kratky, O., Ed.; Academic Press: New York, 1982; p 447.
(20) Hiss, R.; Hobeika, S.; Lynn, C.; Strobl, G. *Macromolecules* **1999**, *32*, 4390.
(21) Hong, K.; Rastogi, A.: Strobl, G. *Macromolecules* **2004**, *37*, 10165.
(22) AI−Hussein, M.; Strobl, G. *Macromolecules* **2002**, *35*, 8515.
(23) Men, Y.; Riger, J.; Hong, K. *J. Polym. Sci., Polym. Phys.* **2005**, *43*, 87.
(24) Men, Y.; Strobl, G. *J. Macromol. Sci., Phys.* **2001**, *40*, 775.
(25) Wu, J.; Schultz, J. M.; Yeh, F.; Hsiao, B. S.; Chu, B. *Macromolecules* **2000**, *33*, 1765.
(26) Takigawa, T.; Urayama, K.; Morino, Y.; Masuda, T. *Polym. J*. **1994**, *25*, 929.
(27) Takigawa, T.; Urayama, K.; Masuda, T. *Polym. Gels Networks* **1994**, *2*, 59.
(28) Takigawa, T.; Morino, Y.; Urayama, K.; Masuda, T. *Polym. J*. **1996**, *28*, 1012.
(29) Urayama, K.; Takigawa, T.; Masuda, T. *Macromolecules* **1993**, *26*, 3092.
(30) Butler, M. F.; Donald, A. M. *Macromolecules* **1998**, *31*, 6234.
(31) Lin, L.; Argon, A. S. *J. Mater. Sci.* **1994**, *29*, 294.
(32) Peterlin, A. *J. Mater. Sci*. **1971**, *6*, 490.
(33) Meinel, G.; Peterlin, A. *J. Polym. Sci., Polym. Phys.* **1971**, *9*, 1967.
(34) Balta-Calleja, F. J.; Peterlin, A. *J. Macromol. Sci., Phys*. **1970**, *B4*, 519.
(35) Young, R. J.; Bowden, P. B.; Ritchie, J. M.; Rider, J. G. *J. Mater. Sci.* **1973**, *8*, 23.
(36) Brady, J. M.; Thomas, E. L. *J. Mater. Sci*. **1989**, *24*, 3311.
(37) Crist, B.; Fisher, C. J.; Howard, P. R. *Macromolecules* **1989**, *22*, 1709.
(38) Fakirov, S.; Fakirov, C.; Fischer, E. W.; Stamm, M. *Polymer* **1991**, *32*, 1173.
(39) Fakirov, S.; Fakirov, C.; Fischer, E. W.; Stamm, M.; Apostolov, A. A. *Colloid Polym. Sci*. **1993**, *271*, 811.
(40) Fakirov, S.; Denchev, Z.; Apostolov, A. A.; Stamm, M.; Fakirov, C. *Colloid Polym. Sci*. **1994**, *272*, 1363.
(41) Stribeck, N.; Sapoundjieva, D.; Denchev, Z.; Apostolov, A. A.; Zachmann, H. G.; Stamm, M.; Fakirov, S. *Macromolecules* **1997**, *30*, 1329.
(42) Liu, L.; Hsiao, B. S.; Fu, B. X.; Ran, S.; Toki, S. Chu, B. Tsou, A. H.; Agarwal, P. K. *Macromolecules* **2003**, *36*, 1920.
(43) Butler, M. F.; Donald, A. M.; Ryan, A. J. *Polymer* **1998**, *39*, 39.
(44) Prevorsek, D. C. *J. Polym. Sci., Part B: Polym. Phys.* **1971**, *32*, 343.
(45) Prevorsek, D. C.; Harget, P. J.; Sharma, R. K.; Reimschuessel, A. C. *J. Macromol. Sci., Phys.* **1973**, *B8*, 127.

MA052595U